BNL-108075-2015-JA

Structure, strain and stability of ultra-thin Ge layers in Si/Ge/Si axial heterojunction nanowires

Cheng-Yen Wen,[1] Mark C. Reuter,[2] Dong Su,[3] Eric A. Stach,[3] Frances M. Ross[2]

[1] Department of Materials Science and Engineering, National Taiwan University, Taipei, Taiwan
[2] IBM T. J. Watson Research Center, Yorktown Heights, NY, USA
[3] Center for Functional Materials, Brookhaven National Laboratory, Upton, NY, USA

Abstract

The abrupt heterointerfaces in the Si/Ge materials system presents useful possibilities for electronic device engineering because the band structure can be affected by strain induced by the lattice mismatch. In planar layers, heterointerfaces with abrupt composition changes are difficult to realize without introducing misfit dislocations. However, in catalytically grown nanowires, abrupt heterointerfaces can be fabricated by appropriate choice of the catalyst. Here we grow nanowires containing Si/Ge and Si/Ge/Si structures respectively with sub-1nm thick Ge "quantum wells" and we measure the interfacial strain fields using geometric phase analysis. Narrow Ge layers show radial strains of several percent, with a corresponding dilation in the axial direction. Si/Ge interfaces show lattice rotation and curvature of the lattice planes. We conclude that high strains can be achieved, compared to what is possible in planar layers. In addition, we study the stability of these heterostructures under heating and eletron beam irradiaition. The strain and composition gradients are supposed to the cause of the instability for interdiffusion.

Semiconductor heterostructures have fascinating applications in band-gap engineering because new physics or extraordinary properties can be created by tuning the lattice-mismatch-induced strain at the interface.[1-3] However, during thin film growth, lattice mismatch often drives the introduction of misfit dislocations, which increase leakage currents and change the designed strain state.[4,a,b] Recent advances in nanofabrication suggest a possible route to overcome the mismatch obstacle. The key is to grow heterojunctions in spatially confined regions such as nanowires, so that the lattice relaxes elastically in the lateral direction, and dislocation introduction is suppressed[c,d]. As well as avoiding misfit dislocations, a second criterion for accurate band-gap engineering is the formation of compositionally abrupt interfaces,[5] since compositional diffuseness will lead to a poorly-defined strain state and band structure. For Group III-V semiconductors, abrupt and dislocation-free heterojunctions have been demonstrated in nanowires grown from catalysts via the vapor-liquid-solid (VLS) process;[6] among others, GaAs/InAs (7% mismatch) and InAs/InP (3% mismatch) heterostructures have been fabricated.[7-9] At these nanowire heterojunctions, the mismatch-induced strain relaxes elastically and misfit dislocations are not observed. In Group IV semiconductors, the nanowire geometry should similarly favor elastic relaxation and suppress misfit dislocations at the Si/Ge interface. However, it has been hard to explore the benefits of nanowire geometry for Group IV heterojunctions, because of an unexpected difficulty in the fabrication of abrupt Si/Ge interfaces in nanowires, known as the "reservoir effect".[10-14] In nanowires grown via the VLS process with conventional AuSi liquid catalysts, compositional changes tend to be diffuse because Si and Ge both have high solubility in the AuSi catalyst. Thus, when the Si source (say) is switched off, a reservoir of Si remains in the catalyst and intermixes with the arriving Ge. The material grown is alloyed, even if the gas flows are changed abruptly.[15-18] One way to address this problem is to choose a catalyst with low Si and Ge solubility.[15] Solid catalysts – $AlAu_2$[19] and AgAu[20] – do indeed improve compositional abruptness in Si/Ge heterointerfaces. By growing nanowires using such catalysts, we now have the opportunity to examine the interfacial structure and quantify the local strain fields in compositionally abrupt Si/Ge interfaces. We can also assess the opportunities for these structures in devices by measuring their stability to thermal or other stimuli.

We have therefore grown two types of Group IV heterostructured nanowires using solid $AlAu_2$ catalysts. For Si/Ge "biwires" (a long Ge segment on a Si nanowire) and Si/Ge/Si tri- or multilayers with ultra-thin (1 nm) Ge layers, we measure the strain fields post-growth using high

resolution electron microscopy. We found that ultrathin Ge layers show radial (in-plane) strains of several percent, with a corresponding dilation in the axial (out of plane) direction, while the biwires show lattice rotation and curvature of the lattice planes at the interface. High strains can therefore be present, compared to what is achievable in planar layers. These strains may be expected to produce strong quantum confinement effects. The stability to heating and to electron irradiation are investigated via *in situ* experiments. We also find that ultra-thin Ge layers are unstable at even relatively low temperature annealing and undergo microstructural rearrangements during electron beam irradiation. This may be due to the extreme strain and concentration gradient, which makes it imperative to control the thermal budget when building these structures into devices.

The Si/Ge heterojunction nanowires were grown in a Hitachi H-9000 ultra-high vacuum transmission electron microscope (UHV-TEM) operated at 300 kV. This microscope has a base pressure of 2×10^{-10} Torr and has been modified so that reactive gases can be flowed into the pole-piece for *in situ* growth observations, and metals can be deposited under UHV by evaporation to serve as catalysts.[21] Each Si(111) sample was flash cleaned in UHV at 1250°C, followed by sequential depositions of Au and Al in a ratio of 2:1. The sample was then resistively heated to 560°C to alloy the metals and react with Si to form liquid $AlAu_2Si$ eutectic catalysts. [111] nanowires with Si/Ge heterojunctions were then grown using a combination of VLS and vapor-solid-solid (VSS) growth modes.[6] First, disilane was flowed at 1×10^{-5} Torr and 560°C to grow Si nanowires with diameters ranging from 20 to 60 nm via the VLS process. Two hours of growth produce 500 nm long nanowires. Then the sample was cooled to typically 385°C to solidify and phase-separate the $AlAu_2Si$ eutectic, forming solid $AlAu_2$. This acts as a catalyst for VSS growth, and growth of Si was continued in the VSS mode for several minutes with a growth rate ~10× slower than the VLS rate. Without changing the temperature, the gas supply was switched to 2×10^{-6} Torr digermane (supplied as 20% digermane in helium) for several minutes to grow a Ge segment, then if desired, switched back to 1×10^{-5} Torr disilane to grow another Si segment. This process could be repeated to form multilayers. After growth, structural analysis at higher spatial resolution was carried out in a C_s-corrected Hitachi HD2700C 200 kV scanning transmission electron microscope (STEM) and a JEOL 3000F 300 kV TEM. In some samples the structural stability was measured in the 300 kV UHV-TEM immediately after growth, without exposure to air. This was done by monitoring contrast changes in the Ge layers

during higher temperature annealing or irradiation by a focused electron beam.

In Figure 1, we show an example of a Si/Ge multilayer nanowire with two different Ge growth times (5 and 2.5 mins). The high-angle annular dark-field STEM (HAADF-STEM) images in Figs. 1(a-b) show intensity proportional to Z^2, where Z is the atomic number; this confirms that solid $AlAu_2$ catalysts can indeed grow sub-1nm Ge layers with apparently abrupt interfaces. A key feature of this image is the registry of the Si and Ge lattices at the interface, with no misfit dislocations visible.

We discuss the strain in this multilayer below, but first we examine the Ge content in more detail by plotting the intensity profile along the growth direction ("out of plane" or z direction) in the inset of Fig. 1(b). Direct examination shows that each Ge layer is two bilayers in thickness. The transition from Si to Ge (measured for the 20-80% contrast change) takes place within three bilayers (< 1 nm). The transition from Ge to Si is less abrupt with interface width of 4 bilayers (> 1 nm). This wider interface implies a somewhat higher solubility of Ge compared to Si in the solid $AlAu_2$ catalyst.[15] This is consistent with thermodynamic calculations of pseudo-binary phase diagrams of $AlAu_2$ with Ge and Si, which show a tendency for the eutectic composition of $AlAu_2$ to contain more Ge than Si.[22] This observation may therefore illustrate the subtle effect of the catalyst reservoir size on the compositional abruptness. Furthermore, the intensity (with respect to Si) of the second (top) Ge layer is somewhat lower than the first (bottom) one. This suggests that for the short Ge growth times used, especially for the second layer, the Ge content may not reach 100%, consistent with the results of the strain analysis below. The increase in Si contrast near the top of the nanowire is due to catalyst material that overlaps the Si, presumably post-growth during cooling or oxidation.

We evaluate the strain distribution at the heterojunctions using geometrical phase analysis (GPA).[23-25] In this technique, a reference area is defined from the high-resolution TEM image, the displacement of the lattice relative to this reference is measured at each point of the image, and a two-dimensional map is calculated showing the relative displacement in the nanowire radial (in-plane, x) and axial (out of plane, z) directions. For Si/Ge heterostructures, note that these maps include two contributions: the intrinsic lattice constant difference due to the presence of Ge (for a $Si_{1-f}Ge_f$ alloy, the intrinsic lattice displacement is proportional to the Ge content ratio f with Δd=0.013f nm), and the actual strain in the lattice. These can be separated only if the fraction of Ge f is known accurately. In Fig. 1(c) we show radial or in-plane relative strain, $\varepsilon_{xx}(x,$

z) = (d-d_{Si})/d_{Si}, and in Fig. 1(d) axial or out of plane relative strain, $\varepsilon_{zz}(x, z)$. Red areas indicate positive strain (expansion) relative to the Si reference (green).

The most striking feature of the radial map in Fig. 1(c) is the lack of strong features at the position of the two Ge layers. At the color scale shown, the map is all the same color, but averaging the numerical values in the x direction shows a small in-plane strain with a broad peak of below 0.5% near the position of the first Ge layer. The lack of a strong modulation in radial strain indicates that the ultra-thin Ge layers are compressed in-plane almost fully to the Si lattice spacing (and conversely, that the Si layers are not much expanded by the Ge). To verify the ability of GPA to quantify such small strains, we simulated lattices with different degrees of strain using the experimental values for pixel size and the parameters used in the GPA Fourier filtering algorithm, finding that strains as small as 0.1% can be measured by GPA.

In contrast, in the axial direction a clear strain is observed (Fig. 1(d)). The measured maximum strains in the axial direction are 3.4% and 2.9% in the first and second Ge layers, respectively, with a smaller strain also extending into the Si above each Ge layer. For a pure Ge layer that is strained in-plane as measured above (i.e. to 0.5% of the Si lattice), we would expect, from the Poisson ratio and lattice mismatch, to observe a lattice strain of 6.9% in the axial direction.[4] The fact that we measure lower values (3.4% and 2.9%) suggests that the Ge may contain some intermixed Si. Ge compositions of respectively 52% and 42% in the two Ge layers in Fig. 1(d) would give maximum strain values that agree with the measurement. Intermixing may also be the origin of the strain observed in the Si regions above each Ge layer, since pure Si with the small in-plane strain discussed above should not show such large out of plane strain. It is difficult to measure the Ge content accurately enough from the HAADF-STEM intensity in Fig. 1(a) to separate the effects of composition and strain more precisely, and the samples damage rapidly if elemental analysis using EDX or EELS is carried out, see below. Nevertheless, we conclude that VSS nanowire growth can produce ultra-thin layers with high Ge content that are almost fully strained in-plane, with corresponding out of plane dilation and no observed dislocations. This stress is expected to lead to band structure changes and carrier confinement effects similar to that predicted for an ideal 1 nm Ge layer embedded in a Si nanowire.[2]

We find that Si/Ge biwire structures can also be grown with sharp compositional gradients and no defects. Figure 2 shows a TEM image of a Si/Ge biwire with a 6 nm thick Ge layer along with GPA measurements of strain and lattice rotation. The contrast in the TEM image in Fig. 2(a)

indicates an abrupt composition change, within 1nm, and perfect lattice registry, i.e. no visible misfit dislocations. Note the presence of Ge on the nanowire surface, more pronounced here than in Fig. 1 due to the longer Ge growth time. This surface Ge causes noise in the strain maps, especially in the lower left corner, but the larger lattice parameter in the Ge segment is still apparent as the red regions in Figs. 2(b, c). In the radial (in-plane) direction, the strain increases monotonically from 0% to ~4% (Fig. 2(b) inset), over a distance of 10nm. This is long relative to the compositional transition. Thus there is a ~5nm region in both Si and Ge in which each material is strained in-plane: the Si is dilated and the Ge compressed by ~2% at the interface. Beyond this transition region, the thick Ge layer has relaxed (radially) almost to its unstrained state. In the out of plane direction, the transition in strain from 0% to ~4% occurs over a shorter distance of ~3nm (Fig. 2(c) inset).

The short lattice parameter transition in the growth direction and longer transition in the radial direction are broadly consistent with finite element calculations. In III-V biwires, such calculations[9] predict a smooth and slow transition for the in-plane lattice parameter, and a sharper but more complex behaviour for the out of plane lattice parameter. Rather than changing in a step function, the out of plane lattice parameter should show a peak on either side of the interface, arising from the Poisson's ratio and the in-plane strain near the interface. In our biwire, this means that the Ge should be dilated out of plane and the Si compressed near the interface. Without carrying out a detailed calculation that includes the 3d nature of the strain field, we could estimate that the 2% in-plane compression measured above for Ge should lead to a 1.5% out of plane dilation just above the interface, and the 2% in-plane dilation for Si should lead to a 1.5% out of plane compression beneath the interface. In the Si, a deep and narrow minimum in out of plane strain can be seen in Fig. 2(c) in the central region just below the interface, but the corresponding effect is not visible in the Ge. It is possible that overgrowth on the Ge section, visible in Fig. 2(a), distorts the strain measurement near the interface. Furthermore, as in the multilayer analysis, interdiffusion may smooth the sharp changes expected for the out of plane lattice parameter. But despite these issues with quantitative interpretation, Fig. 2 confirms that the mismatch-induced coherent strain at the biwire interface distorts both Si and Ge near the heterojunction, with the Ge not recovering to its unstrained state until >~ 3 nm away from the interface. This suggests that a Si/Ge/Si structure with Ge below 6 nm in thickness should be entirely in a compressive strain state.

We conclude that VSS catalysts can form both biwires and thin Ge quantum wells with coherent interfaces and large local strain fields. To make use of these structures in electronic applications, it is necessary to understand their stability during subsequent processing and operation. Indeed, we might expect the combination of high Ge content, high concentration gradients, and large strain to reduce the stability significantly. The thermal stability of epitaxially grown SiGe alloy layers on Si has been studied extensively.[4, 26, 27] Self-diffusion of Ge in SiGe alloys is known to be a function of Ge concentration, and interdiffusion at the SiGe/Si interface is known to be composition-dependent.[26, 27] For example, interdiffusivity is known to increase by 3 orders of magnitude (from ~10^{-17} to 10^{-14} cm^2/s) at 950°C as the Ge fraction increases from 0 to 50%.[26] Strain also has a strong effect on the interdiffusivity, which increases 4.4 times per 0.42% increase of the compressive strain in the SiGe alloy.[27] We evaluated the thermal stability of the ultrathin Ge quantum wells by performing *in situ* annealing on Si/Ge/Si structures in the UHV-TEM immediately after growth. Figure 3 shows a sequence of images after different annealing conditions. At the growth temperature (here 380°C) the as-grown Ge layer appears unchanged after 50 min (Fig. 3(a)). No strong changes are observed even at 490°C for 60 mins (Figs. 3(b-c)). However, after annealing at 530°C for 25 mins, interdiffusion at the Ge layer is clear from the reduced Ge contrast (Fig. 3(d)). Temperatures above 800°C are generally required for significant Si-Ge interdiffusion (for low Ge content alloys).[23] These results show that highly strained high Ge content layers are susceptible to diffusion at temperatures several hundred degrees lower.

We suggest that this low temperature interdiffusion reflects an enhanced role of vacancies. Vacancies are the dominant point defects in Si and Ge at these temperatures, and diffusion experiments and models have shown that vacancies are important to Ge diffusion in SiGe alloys.[28] The large compressive strain in the Ge is expected, from calculations and diffusion models, both to favor the formation of vacancies[29] and to enhance diffusion via vacancies.[30] The relatively large free surface of the Ge layer in a thin nanowire can also enhance diffusion, since the surface is a nearby source for vacancies and possibly an alternative fast diffusion route.

The role of vacancies in mediating diffusion at low temperature can be supported by observing the stability of the Si/Ge/Si structure under electron beam irradiation. Figure 4 shows the results of irradiation with an intense 300 keV electron beam (1500 mA/cm^2, compared to normal imaging at 100 A/cm^2) at 380°C. Voids form in the proximity of the Ge layer, as shown in Fig. 4(c). High-energy electrons are known to generate vacancy-interstitial pairs,[31] and we

suggest that the vacancies may diffuse towards the compressively strained region with sufficient numbers to coalesce into voids. This is analogous to the void formation observed at SiGe/Si interfaces after helium implantation and thermal anneal,[32] where the implantation creates point defects and the anneal drives the vacancies to form voids in the compressively strained (SiGe) region.

In summary, we have grown multilayers, narrow quantum dots and biwires in Si/Ge nanowires using solid $AlAu_2$ catalysts. Lattice distortions measured using geometric phase analysis show that narrow Ge layers can be formed that are almost fully compressed to the Si lattice parameter in-plane and have a corresponding dilation of several percent in the growth direction. In biwires, geometric phase analysis shows that Ge segments can relax fully but only if longer than around 3 nm; thinner Ge layers remain partly strained, and also generate strain in the Si adjacent to the interface. In all the structures grown, the strain fields measured are consistent with some interdiffusion between Si and Ge. Post-growth, we find that further interdiffusion occurs readily, due to the large strains and concentration gradient. The temperatures at which interdiffusion occurs may readily be attained during device processing, making it important to control the thermal budget during post-growth processing of these structures. Nonetheless, the Group IV heterojunction nanowires we have grown provide a prototypical material system that is not easily produced in planar structures, for use in band-gap engineering, as well as for measurement of diffusion and strain relaxation.

Acknowledgements

We acknowledge A. W. Ellis for technical assistance with the UHV-TEM. DS and EAS acknowledge financial assistance from the NSF under Grant No. DMR-0907483. Research was carried out in part at the Center for Functional Nanomaterials, Brookhaven National Laboratory, which is supported by the U.S. Department of Energy, Office of Basic Energy Sciences, under Contract No. DE-AC02-98CH10886.

Figure captions

Figure 1. (a-b) HAADF-STEM image of a heterojunction structure with two Ge layers in a Si nanowire. The growth direction is along the [111] crystallographic axis and the imaging direction is parallel to a <011> direction. Growth took place at 385°C. The first Ge layer was grown with 10^{-6} Torr Ge_2H_6 for 5 minutes, followed by Si grown with 5×10^{-6} Torr Si_2H_6 for 30 minutes. The second Ge layer was grown with 10^{-6} Torr Ge_2H_6 for a shorter time, 2.5 minutes, followed by the growth of a Si capping layer. The inset shows the Ge content via an intensity profile within the indicated area. The interface widths quoted in the text are the distances between 20% and 80% intensity change. Note that the intensity scale is chosen to emphasize the nanowire structure, so the catalyst appears oversaturated. (c-d) GPA measurement of the radial (in-plane) strain ε_{xx}, parallel to the interface, and the axial (out of plane) strain ε_{zz}, parallel to the axis, respectively, of the heterostructure in (b). The maps have the same colour scale so the low strain values in (c) all appear the same colour. The insets in (c-d) show the actual strain values averaged over the width of each strain map.

Figure 2. (a) High-resolution TEM image of a Si/Ge biwire heterojunction. Si growth took place at 1×10^{-5} Torr and 570°C followed by Ge growth at 5×10^{-6} Torr and 380°C for 30 minutes. Note the Ge islands growing on the nanowire surface due to the long growth time of the top Ge segment. (b-c) GPA strain maps of the radial and axial strains ε_{xx} and ε_{zz}. The insets show the strain profiles averaged over the width of each strain map. (d) GPA map of rigid-body rotation of the lattice points relative to the Si reference. The blue and red areas at the ends of the interface indicate two opposite rotation directions of the lattice, clockwise and counter-clockwise, respectively.

Figure 3. *In situ* TEM images of the morphology of a Si/Ge/Si heterojunction nanowire structure during annealing. To minimize beam irradiation effects, the electron beam was blanked between images. (a) The heterostructure is stable after 50 min anneal at 380°C. (b) After 35 min anneal at 430°C. (c) After 1 h anneal at 490°C. The thin Ge layer contrast is still visible but about half the value in (b); see inset. (d) After 25 min anneal at 530°C. The contrast decreases, indicating

diffusion of Ge. The experiment was performed in the UHV-TEM with a vacuum better than 8×10^{-10} Torr.

Figure 4. *In-situ* TEM images of the evolution of a Si/Ge/Si nanowire under intense electron beam irradiation at 1500 mA/cm^2 after (a) 4 min, (b) 18 min, and (c) 30 min at 380°C in a vacuum better than 1.3×10^{-9} Torr. Voids appear at the position of the Ge layer after 30 min irradiation.

References

a Influence of Strain on Semiconductor Thin Film Epitaxy, E.A. Fitzgerald, S. Samavedam, Y.H. Xie, and L.M. Giovane, J. Vacuum Science and Technology A 15, 1048 (1997)
b Changes in electrical device characteristics during the in situ formation of dislocations, F. M. Ross, R. Hull, D. Bahnck, J. C. Bean, L. J. Peticolas, and C. A. King, Appl. Phys. Lett. 62, 1993 1426-1428
c The effect of substrate growth area on misfit and threading dislocation densities in mismatched heterostructures, E. A. Fitzgerald, J. Vac. Sci. Technol. B 7, 782 (1989)
or we could use e.g.
Increased critical thickness for high Ge-content strained SiGe-on-Si using selective epitaxial growth, M. Kim, P. Hashemi, and J. L. Hoyt, Applied Physics Letters 97, 262106 (2010)
There are probably many others; what do you prefer?
d GaN nanostructure design for optimal dislocation filtering; Z. Liang, R. Colby, I. H. Wildeson, D. A. Ewoldt, T. D. Sands, E. A. Stach and R. E. Garcia, J. Appl. Phys. 108, 074313, 2010.

1. Bean, J. C. *Science* **1985,** 230, 127.
2. Swadener, J. G.; Picraux, S. T. *J. Appl. Phys.* **2009,** 105, 044310.
3. Rogers, J. A.; Lagally, M. G.; Nuzzo, R. G. *Nature* **2011,** 477, 45.
4. Kasper, E.; Heim, S. *Appl. Surf. Sci.* **2004,** 224, 3.
5. Lieber, C. *Nano Lett.* **2002,** 2, (2), 81-82.
6. Wagner, R. S.; Ellis, W. C. *Appl. Phys. Lett.* **1964,** 4, 89.
7. Ohlsson, B. J.; Bjork, M. T.; Persson, A. I.; Thelander, C.; Wallenberg, L. R.; Magnusson, M. H.; Deppert, K.; Samuelson, L. *Physica E* **2002,** 13, (2-4), 1126-1130.
8. Björk, M. T.; Ohlsson, B. J.; Sass, T.; Persson, A. I.; Thelander, C.; Magnusson, M. H.; Deppert, K.; Wallenberg, L. R.; Samuelson, L. *Applied Physics Letters* **2002,** 80, (6), 1058-1060.
9. Larsson, M. W.; Wagner, J. B.; Wallin, M.; Håkansson, P.; Fröberg, L. E.; Samuelson, L.; Wallenberg, L. R. *Nanotechnol.* **2007,** 18, 015504.
10. Wu, Y.; Fan, R.; Yang, P. *Nano Letters* **2002,** 2, (2), 83-86.
11. Zakharov, N. D.; Werner, P.; Gerth, G.; Schubert, L.; Sokolov, L.; Gösele, U. *J. Cryst. Growth* **2006,** 290, 6.
12. Dujardin, R.; Poydenot, V.; Devillers, T.; Favre-Nicolin, V.; Gentile, P.; Barski, A. *Appl. Phys. Lett.* **2006,** 89, (15), 153129.
13. Hanke, M.; Eisenschmidt, C.; Werner, P.; Zakharov, N. D.; Syrowatka, F.; Heyroth, F.; Schafer, P.; Konovalov, O. *Physical Review B (Condensed Matter and Materials Physics)* **2007,** 75, (16), 161303.
14. Eisenhawer, B.; Sivakov, V.; Berger, A.; Christiansen, S. *Nanotech.* **2011,** 22, 305604.
15. Li, N.; Tan, T. Y.; Gösele, U. *Appl. Phys. A* **2008,** 90, (4), 591-596.
16. Clark, T. E.; Nimmatoori, P.; Lew, K.-K.; Pan, L.; Redwing, J. M.; Dickey, E. C. *Nano Lett.* **2008,** 8, (4), 1246.
17. Perea, D. E.; Li, N.; Dickerson, R. M.; Misra, A.; Picraux, S. T. *Nano Lett.* **2011,** 11, 3117.
18. Periwal, P.; Sibirev, N. V.; Patriarche, G.; Salem, B.; Bassani, F.; Dubrovskii, V. G.; Baron, T. *Nano Lett.* **2014,** 14, 5140.
19. Wen, C.-Y.; Reuter, M. C.; Bruley, J.; Tersoff, J.; Kodambaka, S.; Stach, E. A.; Ross, F. M. *Science* **2009,** 326, 1247.
20. Chou, Y. C.; Wen, C.-Y.; Reuter, M. C.; Su, D.; Stach, E. A.; Ross, F. M. *ACS Nano* **2012,** 6,

6407.
21. Ross, F. M. *Rep. Prog. Phys.* **2010,** 73, 114501.
22. Jiang, Y. A computational thermodynamic model of Al-Au-Ge-Si quaternary system. The Ohio State University, 2011.
23. Hÿtch, M. J.; Snoeck, E.; Kilaas, R. *Ultramicroscopy* **1998,** 74, 131.
24. Taraci, J. L.; Hytch, M. J.; Clement, T.; Peralta, P.; McCartney, M. R.; Drucker, J.; Picraux, S. T. *Nanotech.* **2005,** 16, 2365.
25. Kim, Y. H.; Park, H. J.; Kim, K.; Kim, C. S.; Yun, W. S.; Lee, J. W.; Kim, M. D. *Appl. Phys. Lett.* **2009,** 95, (033112).
26. Zangenberg, N. R.; Lundsgaard Hansen, J.; Fage-Pedersen, J.; Nylandsted Larsen, A. *Phys. Rev. Lett.* **2001,** 87, (12), 125901.
27. Xia, G.; Hoyt, J. L.; Canonico, M. *J. Appl. Phys.* **2007,** 101, 044901.
28. Cowern, N. B. E.; Zalm, P. C.; Sluis, P. v. d.; Gravesteijn, D. J.; Boer, W. B. d. *Phys. Rev. Lett.* **1994,** 72, 2585.
29. Antonelli, A.; Bernholc, J. *Phys. Rev. B* **1989,** 40, 10643.
30. Aziz, M. J. *Appl. Phys. Lett.* **1997,** 70, 2810.
31. Williams, D. B.; Carter, C. B., *Transmission Electron Microscopy*. 2nd ed.; Springer: 2009.
32. D'Angelo, D.; Mirabella, S.; Bruno, E.; Terrasi, A.; Bongiorno, C.; Giannazzo, F.; Raineri, V.; Bisognin, G.; Berti, M. *J. Appl. Phys.* **2008,** 103, 016104.

Figure 1

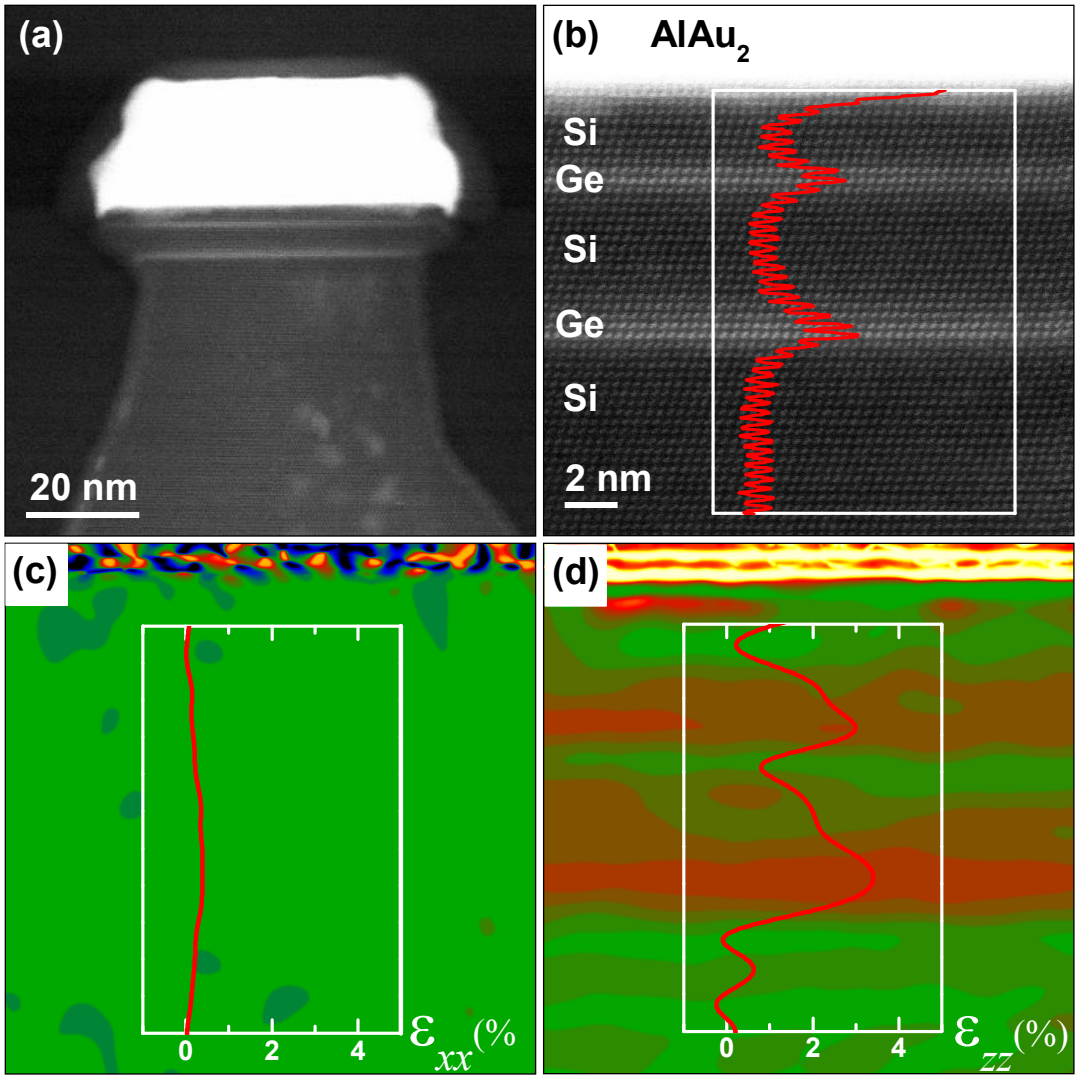

Figure 2

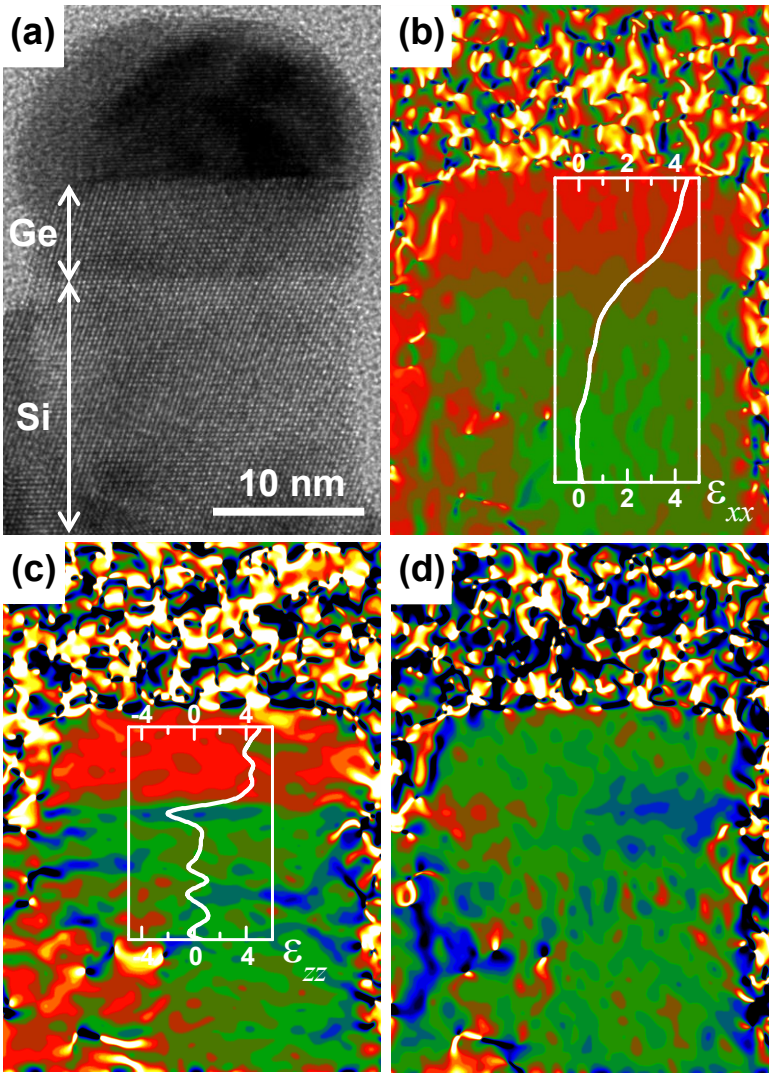

20 nm

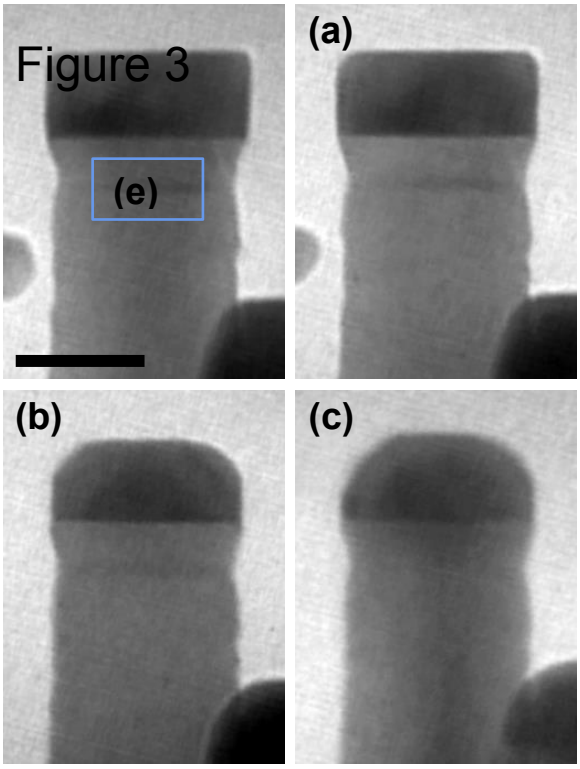
Figure 3
(e)
(a)
(b)
(c)

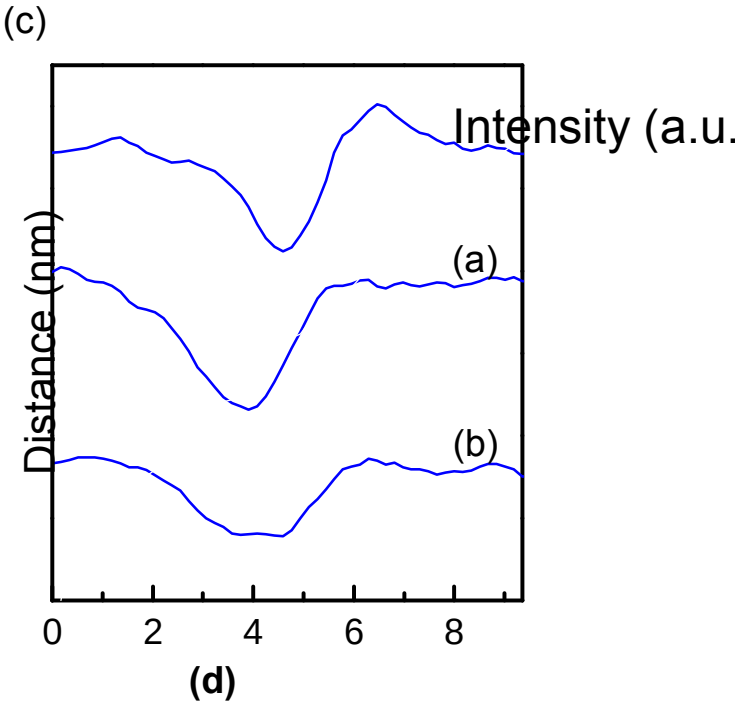
(c)
Intensity (a.u.
Distance (nm)
(a)
(b)
0
2
4
6
8
(d)

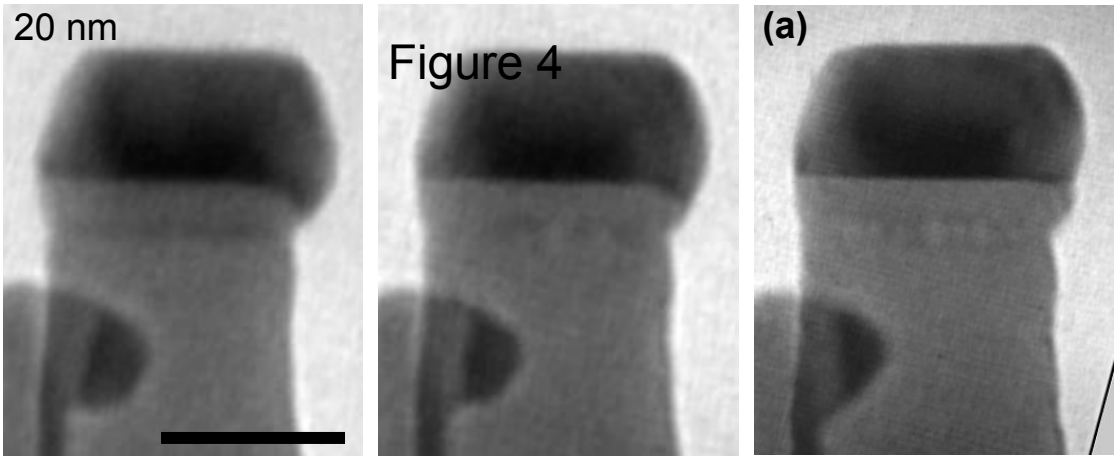
20 nm
Figure 4
(a)